On the method of photoconductive detection of defects in semiconductors by vibrational mode-related Fano resonances

F. Herklotz,[1] I. Chaplygin,[1] and E. V. Lavrov[1,2]
[1]*Technische Universität Dresden, 01062 Dresden, Germany*
[2]*Tomsk State University, 634050 Tomsk, Russia*

(Received 24 April 2018; accepted 21 June 2018; published online 13 July 2018)

The method of photoconductive detection of defect-related vibrational modes in semiconductors by Fano resonances is validated by a combined photoconductivity and infrared absorption study of the interstitial hydrogen donor in ZnO. Depth-resolved isotopic substitution experiments with varying concentrations of H and D show that the effect of vibrational mode-related absorption has to be taken into account in order to allow for an unambiguous interpretation of the experimental data. A quantitative model is presented which describes the influence of sample thickness, defect concentration, and the presence of other donors on the sign, magnitude, and shape of the Fano resonances. Implications for the photoconductive detection of defect-related vibrational modes are discussed. *Published by AIP Publishing*. https://doi.org/10.1063/1.5037412

I. INTRODUCTION

The identification and characterization of light impurities in semiconductors by means of local vibrational mode (LVM) spectroscopy became an important experimental approach ever since semiconductors were recognized as technologically important materials. The knowledge about the vibrational spectrum of defect complexes provides a wealth of information about their chemical composition, symmetry, thermal stability, etc.[1] From an experimental point of view, however, the standard methods of probing LVMs, like infrared (IR) absorption or Raman scattering, have three major limitations: (i) they fail if the vibrational mode frequency occurs in a strongly absorbing/reflecting spectroscopic region of the semiconductor crystal, (ii) the sensitivity of these techniques is often too low to obtain useful information, and (iii) the defect's electrical activity in most cases remains unknown because frequencies of LVMs are rather insensitive to the defect's charge state.

In order to address these challenges, the method of photoconductive (PC) detection of LVMs has been recently proposed.[2–5] The basic principle of this technique is an interaction of vibrational excitations with the continuum of electronic states in the conduction/valence band resulting in the appearance of Fano resonances in the photoconductivity spectra (see Fig. 1 in Ref. 4). The benefits of PC-based vibrational mode spectroscopy have been demonstrated on: (i) hydrogen substituting for oxygen in ZnO, where its LVM occurs in the highly absorbing multi-phonon region,[2] (ii) interstitial oxygen in ultra-thin Si films, which illustrates exceptionally high sensitivity,[5] and (iii) interstitial hydrogen in ZnO and rutile TiO_2, from which the shallow donor nature of these defects was concluded.[3,4]

The shape of the Fano resonance, *Fanian*,[6] is given by

$$I(\epsilon) \propto \frac{(\epsilon + q)^2}{1 + \epsilon^2}, \quad \epsilon = \frac{\omega - \Omega_0 - \Delta\Omega}{\Gamma/2}, \tag{1}$$

where Ω_0 is the LVM frequency, Γ is the spectral width, $\Delta\Omega$ is the additional shift, and q is the line shape parameter. Qualitatively, the shape of the resonance strongly depends on q ranging from an antiresonance ($q = 0$) to a Lorentzian ($q \to \pm\infty$). The latter case manifests itself as an enhancement of the photocurrent at $\omega \approx \Omega_0$ with respect to the background, which unambiguously implies that the corresponding defect is a dominant donor/acceptor in the sample. Thus, photoconductive detection of LVM provides not only the means to detect defects in the cases where the standard techniques fail, but equally importantly, allows to unveil their electrical activity.

The shape and even the *sign* of the Fano resonances, however, critically depend not only on the nature of the defect but also on the cumulative impact of defect's concentration, the sample thickness, and the presence of other donors/acceptors contributing to the photocurrent.[4]

While there is a qualitative understanding of the basics of photoconductive detection of LVMs, a quantitative model explaining the sign, the shape, and the magnitude of the corresponding Fano resonances is still lacking. Here, we present the results of a detailed photoconductivity and IR absorption study of bond-centered interstitial hydrogen (H_{BC}) acting as a shallow donor in ZnO.[7–9] With this well-known probe system, we show how the apparent shape of the Fano resonances due to the vibrational excitations of H_{BC} and its isotopic counterpart D_{BC} depend on the donor's concentration, the sample thickness, and the amount ratio between hydrogen and deuterium.

II. EXPERIMENTAL DETAILS

ZnO samples used in the present study were nominally undoped needle-shaped single crystals grown from the vapor phase at the Institute for Applied Physics, University of Erlangen, Germany and had dimensions of about $10 \times 3 \times 2\,mm^3$. Hydrogen or/and deuterium was/were introduced into the samples via thermal treatments in closed quartz

ampules filled with H_2, D_2 or a gas mixture of H_2 and D_2 ($[H_2]/[D_2] \approx 1{:}1$). The treatments were performed at 730 °C for 1 h and terminated by quenching the ampules to room temperature in water.

Fourier transform infrared absorption and photoconductivity spectra were recorded with a Bomem DA3.01 Fourier spectrometer equipped with a globar light source and a KBr beam splitter. The incoming light was unpolarized with the wave vector, $\boldsymbol{k}$, directed perpendicular to the $\boldsymbol{c}$ axis of the samples. The spectral resolution was 0.5 and 1 cm^{-1} for the absorption and photoconductivity measurements, respectively. The temperature of the samples during the measurements was stabilized within 1 K in the range of 7–13 K.

For photoconductivity measurements, the ZnO samples were first etched with orthophosphoric acid for 2 min at room temperature. Ohmic contacts with an area of about $2 \times 1\ mm^2$ were then generated by scratching a mixture of an In-Ga alloy onto the sample surface. Contacts were located on the illuminated face of the samples. In order to probe the dependences of the IR and PC signals discussed in the paper on the sample thickness, measurements were performed in a series of mechanical polishing, which gradually thinned down the samples along the $[11\bar{2}0]$ axis. Here, ohmic contacts were located on the freshly polished surface.

III. RESULTS AND DISCUSSION

A. Dependence on the sample thickness

First, we consider the influence of sample thickness on the sign and intensity of Fano resonance due to a local vibrational mode in the photoconductivity spectra. As mentioned in Sec. I, interstitial hydrogen in ZnO acting as a shallow donor has been employed as a probe system. The properties of H_{BC} and its isotopic counterpart D_{BC} in ZnO have been documented in many publications. Both H_{BC} and D_{BC} are effective-mass like shallow donors with an ionization energy of about 53 meV.[9] Spectroscopic features of H_{BC} and D_{BC} were observed in photoluminescence,[10] Raman scattering,[9,11] photoconductivity,[3,4] and IR absorption measurements.[8,9]

Contrary to the electronic properties, vibrational excitations of hydrogen strongly depend on its mass. The stretch LVM of H_{BC} has a frequency of 3611 cm^{-1}. It originates from the defect's O–H bond aligned parallel to the $\boldsymbol{c}$ axis of the crystal.[8] The corresponding LVM frequency of D_{BC} is red-shifted by about a factor of $\sqrt{2}$ down to 2668 cm^{-1}.

The formation of H_{BC} and D_{BC} in ZnO with almost homogeneous solubility-limited concentration profiles for the samples with thicknesses of a few mm can be easily achieved via thermal treatments in H_2 and/or D_2 gas at temperatures above 700 °C.[9,12]

Figure 1 shows exemplary transmission and photoconductivity spectra obtained for a ZnO sample hydrogenated in the mixture of H_2 and D_2 at 730 °C. The spectra were recorded after each step of a mechanical polishing series which gradually reduced the sample thickness from 1800 to 265 μm. The features at 3611 and 2668 cm^{-1} are due to the local vibrational modes of H_{BC} and D_{BC}, respectively. As

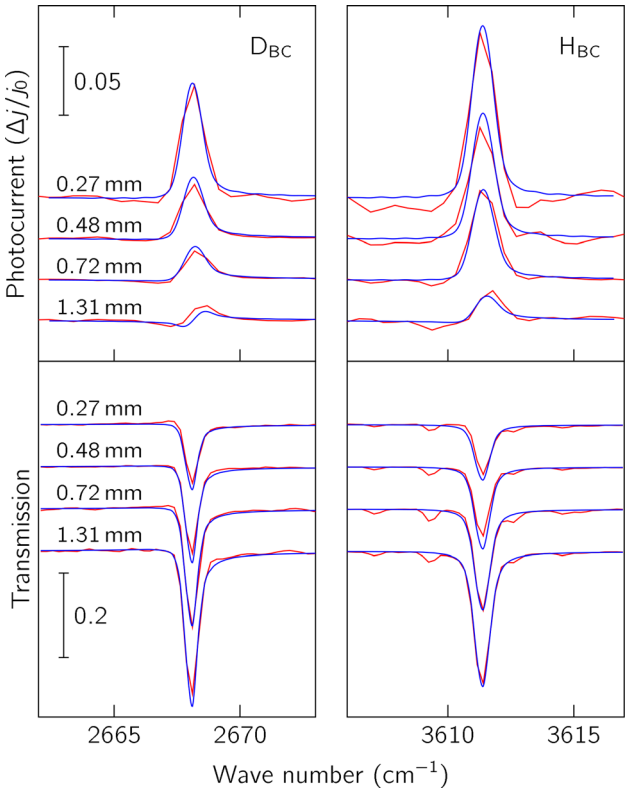

FIG. 1. Sections of photoconductivity and transmission spectra (both red) obtained in a polishing series of a ZnO sample hydrogenated in an $H_2 + D_2$ mixture ambient at 730 °C for 1 h. Spectra are baseline corrected and vertically offset for clarity. The blue lines represent best-fit curves to the experimental data (see Sec. III D).

the sample is thinned down, the intensities of both LVMs in transmission spectra decrease together with the number of absorbing species.

In accordance with earlier studies, the vibrational excitations of H_{BC} and D_{BC} in photoconductivity spectra occur as positive Fano resonances due to the interaction with the continuum of the electronic states in the conduction band of ZnO.[3,4] Counterintuitively, both resonances turned out to become stronger upon the reduction of the sample thickness (upper two panels in Fig. 1).

Figure 2 summarizes the results obtained from the mechanical polishing series. The top panel gives intensities of the Fano resonances due to LVMs of H_{BC} and D_{BC} with respect to the background photocurrent, $\Delta j/j_0$, as a function of sample thickness. The bottom panel shows the thickness dependence of the integrated absorption of the 3611 and 2668 cm^{-1} lines. Generally, the concentration profiles of H_{BC} and D_{BC} can be deduced by multiplying the derivatives of these functions with the corresponding calibration factors given in Ref. 9. Here, the concentration profiles of H_{BC} and D_{BC} along the polishing direction were fitted by superpositions of two asymmetric complementary error functions with maxima at each of the opposite faces of the sample. While the actual concentration profiles may deviate from the computed ones because of substantial error bars in the absorption data, we found that this model results in a reasonably good fit to the experimental data (lines in the bottom panel of the figure).

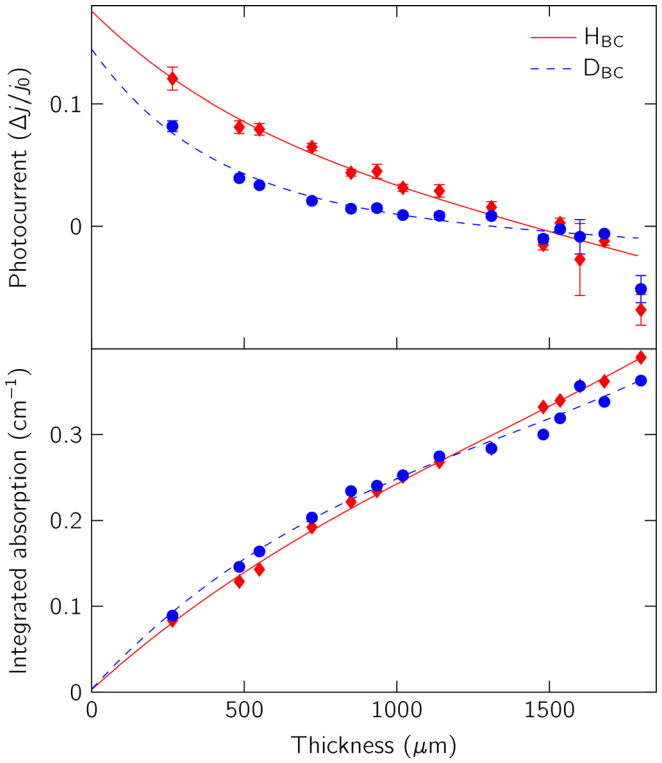

FIG. 2. Photocurrent (top) and integrated absorption (bottom) due to the LVMs of H_{BC} and D_{BC} as a function of the sample thickness. The data were obtained as a result of a mechanical polishing series on a ZnO sample hydrogenated in an $H_2 + D_2$ mixture ambient at 730 °C for 1 h. The red solid and dashed blue lines represent best-fit curves to the experimental data (see the text).

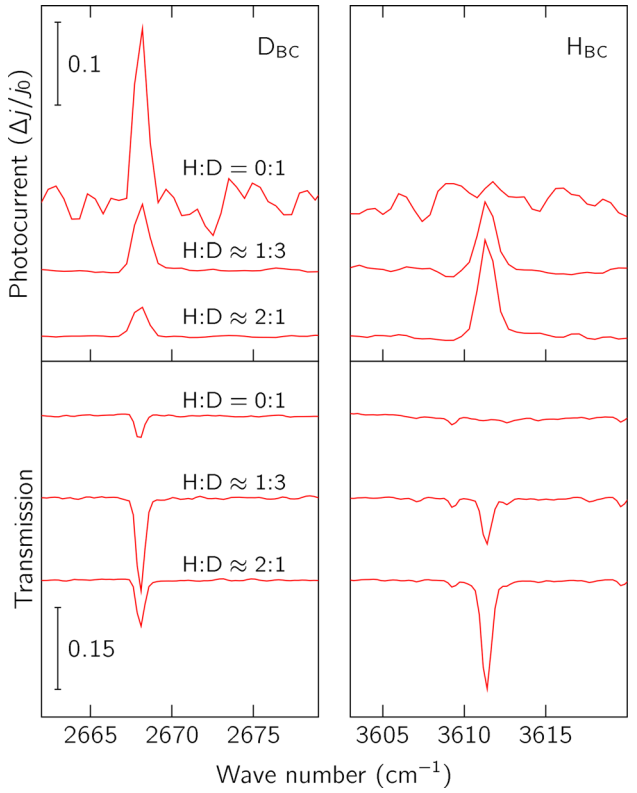

FIG. 3. Sections of photoconductivity and transmission spectra of ZnO samples treated in a hydrogen gas ambient with different H:D ratios. Sample thicknesses: bottom—330 μm, mid—310 μm, and top—90 μm. The spectra are offset vertically for clarity.

The model employed to obtain the best-fit curves to the photocurrent data in the top panel will be explained in detail in Sec. III C.

B. Dependence on the concentration ratio

It has been shown earlier that both sign and intensity of the Fano resonance strongly depend on the concentration ratio of the two (or more) shallow donors present in the sample.[4] Exemplary photoconductivity and transmission spectra for samples treated in strongly different H:D ambients are presented in the upper and lower panel of Fig. 3, respectively. All samples were polished down to about 300 μm in order to minimize the effect of LVM absorption on the Fano resonance peak intensities in the PC spectra. The top PC spectrum was recorded for a sample that has been treated in D_2 gas alone, whereas the two lower spectra were recorded on the samples with the H:D ratios of about 1:3 and 2:1. As can be seen from the figure, the magnitude of the Fano resonance peaks of D_{BC} decreases as the relative amount of H_{BC} grows in. Such a behavior is expected since the contribution of the H_{BC} donors to the net photocurrent becomes dominating.

C. Model

In order to explain the experimental results presented in Secs. III A and III B, we consider a semiconductor with two donors (subscripts e and q) one of which (e) has a local vibrational mode with an energy E_s resulting in a Fano resonance of the corresponding photoconductivity spectrum with a $|q| \gg 1$ or $\gamma \gg q$ (see Sec. III D and the Appendix), whereas the second donor (q) does not have a singularity at E_s (see Fig. 4).

The amount of photoelectrons δn and thus the net photocurrent δj generated by an infinitesimally thin section of a sample along the optical path is the sum of contributions from both donors

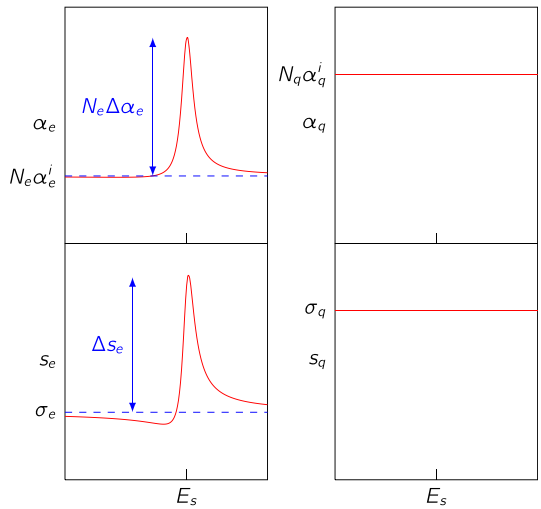

FIG. 4. IR absorption (top) and photoionization cross-section (bottom) of two donors one of which (left) has a local vibrational mode at E_s, whereas the other one (right) does not have a singularity in the vicinity of E_s.

$$\delta j \propto \delta n \propto \left[N_e s_e(E) + N_q s_q(E)\right] dJ dx, \tag{2}$$

where $N_{e,q}$ are the concentrations of the two donors, $s_{e,q}$ are the cross-sections of ionization, and $dJ = IdE$ is the photon flux per energy interval. In order to get an analytic expression for the intensity of Fano resonance, we assume that the concentration profiles $N_{e,q}$ are constant across the sample thickness. In this case, the photon flux is given by

$$I = I_0 \exp(-\alpha(E)x), \tag{3}$$

where $\alpha(E)$ is the absorption coefficient. Integrating Eq. (2) over the sample thickness, we obtain

$$j \propto \left[N_e s_e(E) + N_q s_q(E)\right] \frac{1 - \exp(-\alpha(E)d)}{\alpha(E)}. \tag{4}$$

Here, we are interested in the relative intensity of the e-donor's Fano peak at its resonance frequency E_s with respect to the background

$$\frac{\Delta j}{j_0} = \frac{j(E_s) - j(E \neq E_s)}{j(E \neq E_s)}. \tag{5}$$

Generally, the frequency-dependent absorption coefficient $\alpha(E)$ is a sum of those due to lattice absorption and the two shallow donors. Disregarding for the sake of simplicity the contribution of the lattice, we get that

$$\begin{aligned} \alpha(E_s) &= N_e(\alpha_e^i + \Delta\alpha_e) + N_q\alpha_q^i, \\ \alpha(E \neq E_s) &= N_e\alpha_e^i + N_q\alpha_q^i. \end{aligned} \tag{6}$$

Here, $\alpha_{e,q}^i$ is a term independent of E, whereas $\Delta\alpha_e$ is the LVM absorption strength at E_s. Similarly, the ionization cross-sections can be described by

$$\begin{aligned} s(E_s) &= \sigma_e + \Delta s_e + \sigma_q, \\ s(E \neq E_s) &= \sigma_e + \sigma_q, \end{aligned} \tag{7}$$

where $\sigma_{e,q}$ are independent of E, whereas Δs_e represents the additional term in the ionization cross-section due to the Fano resonance.

In our model, we assume that both shallow donors can be described by the effective-like mass theory, which implies that (see Ref. 13)

$$\sigma_e = \sigma_q \equiv \sigma, \tag{8}$$

$$\alpha_e^i = \alpha_q^i \equiv \alpha_i = \frac{5.26 \times 10^{-17}\text{cm}^{-2}}{n_r} \frac{m}{m^*} \frac{E_\text{H}}{E_i} \left(\frac{E_i}{E}\right)^{3.5}, \tag{9}$$

where n_r is the refractive index, $E_\text{H} = 13.6\,\text{eV}$ is the ionization energy of hydrogen, E_i is the ionization energy of the shallow donors, and m and m^* are the mass of a free electron and its effective mass in the crystal, respectively. For H_{BC} (D_{BC}) in ZnO with $E_i = 53\,\text{meV}$, $m^*/m = 0.3$,[14–16] and $n_r = 1.9$,[17] we obtain that α_i is about $1.35 \times 10^{-17}\,\text{cm}^2$ (3.88×10^{-17} cm^2) at $3611\,\text{cm}^{-1}$ ($2668\,\text{cm}^{-1}$). The LVM absorption strength at E_s is deduced from the absorption data giving $\Delta\alpha_e \approx 4.3 \times 10^{-17}(2.3 \times 10^{-17})$ cm^{-2} for H_{BC} (D_{BC}). It follows from here that $\Delta\alpha_e/\alpha_i \approx 3.22$ (0.59) for H_{BC} (D_{BC}).

Finally, from Eqs. (4) and (5), we obtain the intensity of the resonance in a sample doped with two shallow donors

$$\frac{\Delta j}{j_0} = \frac{1 + \eta + \eta\Delta s_e/\sigma}{1 + \eta + \eta\Delta\alpha_e/\alpha_i} \times \frac{1 - \exp\left(-N_q[1 + \eta + \eta\Delta\alpha_e/\alpha_i]\alpha_i d\right)}{1 - \exp\left(-N_q[1 + \eta]\alpha_i d\right)} - 1, \tag{10}$$

where $\eta \equiv N_e/N_q$.

It follows from Eq. (10) that in the case of thin films, ($d \to 0$)

$$\frac{\Delta j}{j_0} = \frac{\eta}{1 + \eta} \frac{\Delta s_e}{\sigma}. \tag{11}$$

In particular, for two donors with equal concentrations ($\eta = 1$), the signal is half as strong as in the case of a single donor ($\eta \to \infty$).

For thick samples ($d \to \infty$), we have

$$\frac{\Delta j}{j_0} = \eta \frac{\Delta s_e/\sigma - \Delta\alpha_e/\alpha_i}{1 + \eta + \eta\Delta\alpha_e/\alpha_i}. \tag{12}$$

As one can see, the sign of the resonance for thick samples depends on the difference $\Delta s_e/\sigma - \Delta\alpha_e/\alpha_i$. That is, regardless of the thickness, for a LVM with weak oscillator strength, ($\Delta\alpha_e/\alpha_i \to 0$) the resonance remains positive. Otherwise, not only the magnitude but also the sign of the resonance depends on d, N_e, and N_q. Moreover, at some stage, it becomes zero and disappears from the spectra.

Figure 5 shows intensities of the Fano resonances due to the LVMs of the H_{BC} and D_{BC} donors in the photoconductivity spectra of ZnO calculated from Eq. (10). In both cases, the concentration of q-donor was set to $10^{17}\,\text{cm}^{-3}$. The black line separates regions with positive and negative resonances.

Equation (10) cannot be directly employed to fit the experimental data presented in Fig. 2 since the concentrations of interstitial hydrogen and deuterium are not constant. The lines in the top panel of Fig. 2 show the curves with the best-fit values $\Delta s_\text{H}/\sigma_{3611} = 0.55 \pm 0.12$ and $\Delta s_\text{D}/\sigma_{2668} = 0.34 \pm 0.09$ obtained from a numerical fitting procedure with the concentration profiles explained in Sec. III A. Obviously, our model can explain the experimental results reasonably well. Note that the same values of $\Delta s_e/\sigma$ were taken to calculate the surfaces presented in Fig. 5.

In the end of this section, we comment on the photoconductivity data obtained on the unpolished sample. The points at 1800 μm in the top panel of Fig. 2 do not seem to match the best-fit curves. We explain this mismatch by the formation of other shallow donors which is known to take place in the near-surface layer of ZnO in the course of the hydrogenation treatment. Well-known candidates are hydrogen and deuterium substituting for oxygen (H_O and D_O), which form shallow donor states in the band gap with an ionization energy of 47 meV.[9] Under conditions employed in this work, it is H_O (D_O) rather than H_{BC} (D_{BC}) that is the dominant donor(s) in a 5 μm-thick near-surface layer of the sample.[10,18] The effect of H_O and/or D_O would be therefore similar to that of the q-donor discussed above, that is, the photocurrent due to H_O and D_O

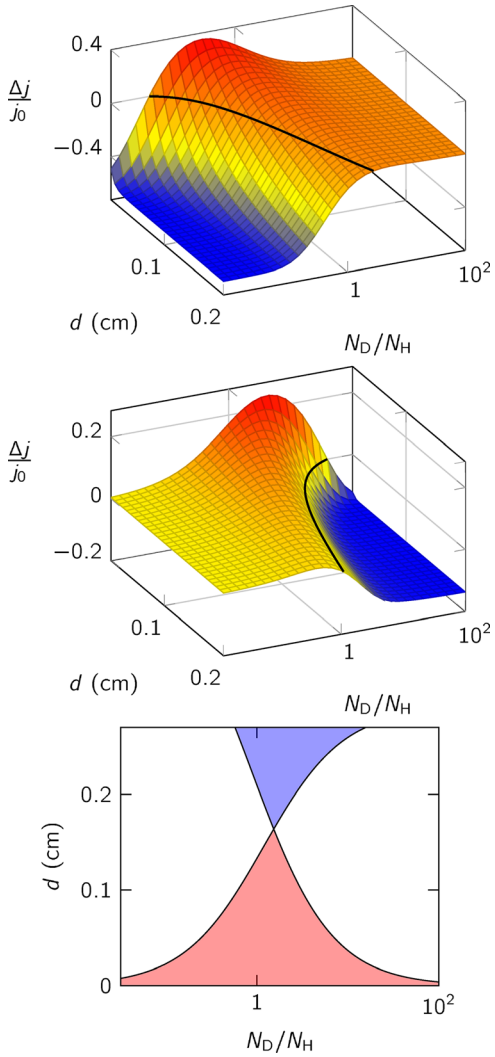

FIG. 5. Calculated intensities of Fano resonances due to LVMs of H_{BC} (top) and D_{BC} (mid) as a function of sample thickness and concentration ratio N_D/N_H. The black lines denote parameters at which the resonances disappear. The bottom figure shows a 2D map of parameters d and N_D/N_H at which resonances are both positive (red), both negative (blue) or have opposite sign (white). The concentration of the q-donor (see the text) is set to $10^{17}\,cm^{-3}$.

"competes" with that of the e-donor making the H_{BC} and D_{BC} Fano resonance features more negative. The magnitude of this effect should be strongly dependent on the particular measurement geometry, concentration profiles, etc., and is not considered here quantitatively.

D. Shape of Fano resonances

As evident from Fig. 1, not only the amplitude but also the shape of the Fano resonance features in photocurrent change with the sample thickness for both H_{BC} and D_{BC}. The classical formula given by Eq. (1) cannot be employed to fit the spectra presented in Fig. 1 since it predicts zero photocurrent at $\epsilon = -q$, which is never observed experimentally. The generalized shape given by (for the derivation, see Appendix A)

$$I(\epsilon) \propto \frac{(\epsilon+q)^2+\gamma}{\epsilon^2+1}, \quad \epsilon = \frac{\omega-\Omega_0-\Delta\Omega}{\Gamma/2}, \tag{13}$$

TABLE I. Best-fit parameters for ionization cross-section s_e and IR absorption $\Delta\alpha$ at LVMs of H_{BC} and D_{BC}.

	s_e		$\Delta\alpha$	
	H_{BC}	D_{BC}	H_{BC}	D_{BC}
q	0.019	0.029	0.058	0.079
γ	1.9	1.9	3.8	2.0

with an additional parameter γ was used to approximate ionization cross sections $s_e(E)$ and absorption curves $\Delta\alpha(E)$ due to LVMs of interstitial hydrogen and deuterium. The instrumental resolution of the Fourier spectrometer was taken into account as well. The best-fit spectra are presented by the blue lines in Fig. 1. Note that the minor features around the $3611\,cm^{-1}$ line, for instance at 3609 and $3612.5\,cm^{-1}$, are due to residual water vapor in the spectrometer. The good agreement between experimental data and simulated spectra gives us confidence in the validity of our model. The best-fit parameters q and γ are gathered in Table I.

It follows from the table that in all cases, $\gamma \gg q$, which implies that Fano resonances due to H_{BC} and D_{BC} have basically a Lorentzian shape. The apparent asymmetry of the peaks especially obvious for large sample thicknesses is a result of the distortion caused by the absorption as discussed in Sec. III C. We also note that both q and γ are slightly larger for IR absorption than in the case of photoconductivity. This finding is in qualitative agreement with the theoretical consideration given in the Appendix [see Eq. (B3)].

IV. SUMMARY

A combined photoconductivity and IR absorption study of the interstitial hydrogen donor in ZnO is presented. With the help of this probe system, it is shown that the sign, intensity, and shape of Fano resonances due to vibrational excitations of shallow donors occurring in the photoconductivity spectra strongly depend on the sample thickness and the presence of other electrically active impurities. The distortion of the "natural" Fano shape of the resonances for bulk samples is explained by the competing processes of photoionization and absorption at the frequency of the corresponding local vibrational mode. A quantitative model explaining all the experimental results is proposed.

ACKNOWLEDGMENTS

This work was funded by the Deutsche Forschungsgemeinschaft (Grant No. LA 1397/10). E.V.L. acknowledges the support by the Tomsk State University Competitiveness Improvement Program (Project No. 8.2.22.2018). We are also grateful to T. Mchedlidze (Technische Universität Dresden) for the help with the sample preparation. V. V. Melnikov (Tomsk State University) is acknowledged for reading through the manuscript and providing useful comments.

APPENDIX A: PHOTOCONDUCTIVITY

Consider a photoconductivity spectrum of a defect (i.e., shallow donor) which has an additional electrically inactive localized state (i.e., vibrational mode) coupled with two continua: one resulting in a photocurrent via transition operator $\hat{T}_e$, whereas for the other one, the transitions from the ground state into the conduction or valence band are forbidden (see Fig. 6).[19] Our analysis is based on the formalism reported in Refs. 20–23. A similar approach has been applied earlier to study photoconductivity spectra due to resonant electron-phonon interaction in Si.[24]

The photocurrent is given by

$$I(E) = \sum_{E'} |\langle g|\hat{T}_e|E'\rangle|^2 \delta(E-E') = \langle g|\hat{T}_e \left(\sum_{E'} |E'\rangle\delta(E-E')\langle E'|\right)\hat{T}_e|g\rangle, \quad \text{(A1)}$$

with

$$\sum_{E'} \delta(E-E') = -\frac{1}{\pi} Im \sum_{E'} \langle E'|\hat{G}|E'\rangle, \quad \text{(A2)}$$

where $\hat{G}$ is the resolvent or Green's operator of the system

$$\hat{G} = \frac{1}{E-\hat{H}+i\epsilon}. \quad \text{(A3)}$$

Here,

$$\hat{H} = \hat{H}_e + \hat{H}_q + \hat{H}_s + \hat{W} + \hat{V} \equiv \hat{H}_0 + \hat{W} + \hat{V}, \quad \text{(A4)}$$

where $\hat{H}_e$ is a Hamiltonian of the first continuum interacting with the localized state $|s\rangle$ via operator $\hat{V}$, $\hat{H}_q$ is a Hamiltonian of the second continuum interacting with the $|s\rangle$ state via operator $\hat{W}$, so that the matrix elements are independent of the $|e\rangle$ and $|q\rangle$ states and are equal to V and W, respectively. With Eq. (A2), the photocurrent given by Eq. (A1) can be rewritten as

$$I(E) = -\frac{1}{\pi} Im\langle g|\hat{T}_e\hat{G}\hat{T}_e|g\rangle. \quad \text{(A5)}$$

Here, we used the property of completeness and orthogonality of both perturbed $|E'\rangle$ and unperturbed $|s\rangle$, $|e\rangle$, $|q\rangle$ basis sets

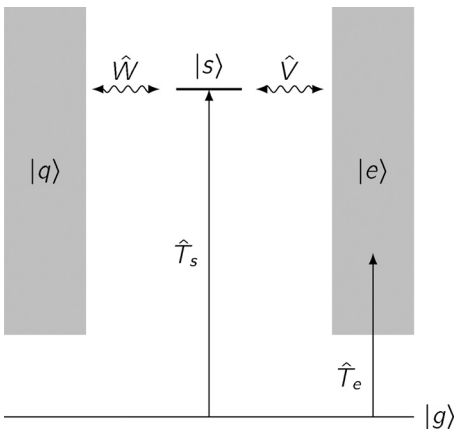

FIG. 6. Energy level diagram of a model system giving rise to a Fano resonance in photoconductivity and IR absorption spectra.

$$\hat{1} = \sum_{E'} |E'\rangle\langle E'| = |s\rangle\langle s| + \sum_e |e\rangle\langle e| + \sum_q |q\rangle\langle q| \quad \text{and} \quad \langle i|i\rangle = 1. \quad \text{(A6)}$$

Since the transition operator $\hat{T}_e$ acts only between the ground state and the electronic states $|e\rangle$, it is more convenient to rewrite Eq. (A1) in the unperturbed basis set as

$$I(E) = -\frac{1}{\pi} Im\langle g|\hat{T}_e\hat{G}\hat{T}_e|g\rangle = -\frac{1}{\pi}\sum_{e',e''}\langle g|\hat{T}_e|e'\rangle\langle e'|\hat{G}|e''\rangle\langle e''|\hat{T}_e|g\rangle. \quad \text{(A7)}$$

We also assume that matrix elements $\langle g|\hat{T}_e|e\rangle$ are real, independent of e, and equal to $T_e = \langle g|\hat{T}_e|e\rangle$, where $|e\rangle$ are the states of the continuum generating photocurrent. This implies that

$$I(E) = -\frac{T_e^2}{\pi} Im \sum_{e',e''}\langle e'|\hat{G}|e''\rangle. \quad \text{(A8)}$$

Further on,

$$\hat{G} = \hat{G}_0 + \hat{G}_0(\hat{V}+\hat{W})\hat{G}, \quad \hat{G}_0 \equiv \frac{1}{E-\hat{H}_0+i\epsilon}. \quad \text{(A9)}$$

In order to get the photocurrent spectrum $I(E)$, we have to calculate the quantity

$$\langle e'|\hat{G}|e''\rangle = \langle e'|\hat{G}_0|e''\rangle + \langle e'|\hat{G}_0(\hat{V}+\hat{W})\hat{G}|e''\rangle. \quad \text{(A10)}$$

Because the $|e\rangle$ states do not interact with $|q\rangle$, we further obtain

$$\langle e'|\hat{G}|e''\rangle = \frac{\delta_{e',e''}}{E-E_{e''}+i\epsilon} + \frac{\langle e'|\hat{V}|s\rangle\langle s|\hat{G}|e''\rangle}{E-E_{e'}+i\epsilon}. \quad \text{(A11)}$$

Performing the summation, we get

$$\sum_{e',e''}\langle e'|\hat{G}|e''\rangle = (R_e - i\pi\rho_e)\left(1 + V\sum_{e''}\langle s|\hat{G}|e''\rangle\right), \quad \text{(A12)}$$

where we used the identity

$$\sum_k \frac{1}{E-E_k+i\epsilon} = R(E) - i\pi\rho(E), \quad \text{(A13)}$$

with $\rho(E)$ being the density of states and $R(E)$ being defined as

$$R(E) = P\int \frac{\rho(E')}{E-E'}dE'. \quad \text{(A14)}$$

Here, P stands for "principal value".

Next, we need to calculate the quantity

$$\langle s|\hat{G}|e'\rangle = \langle s|\hat{G}_0|e'\rangle + \langle s|\hat{G}_0(\hat{V}+\hat{W})\hat{G}|e'\rangle = \frac{\langle s|\hat{V}\hat{G}|e'\rangle}{E-E_s} + \frac{\langle s|\hat{W}\hat{G}|e'\rangle}{E-E_s} = \frac{V}{E-E_s}\sum_{e''}\langle e''|\hat{G}|e'\rangle + \frac{W}{E-E_s}\sum_q\langle q|\hat{G}|e'\rangle. \quad \text{(A15)}$$

The last term above is

$$\begin{aligned}\langle q|\hat{G}|e'\rangle &= \langle q|\hat{G}_0|e'\rangle + \langle q|\hat{G}_0(\hat{V}+\hat{W})\hat{G}|e'\rangle \\ &= \frac{W}{E-E_q+i\epsilon}\langle s|\hat{G}|e'\rangle, \\ \sum_q \langle q|\hat{G}|e'\rangle &= (R_q - i\pi\rho_q)W\langle s|\hat{G}|e'\rangle.\end{aligned} \tag{A16}$$

If we denote

$$\begin{aligned}x &= \sum_{e'}\langle s|\hat{G}|e'\rangle, \\ y &= \sum_{e',e''}\langle e''|\hat{G}|e'\rangle = \sum_{e',e''}\langle e'|\hat{G}|e''\rangle, \\ z &= \sum_{q,e'}\langle q|\hat{G}|e'\rangle.\end{aligned} \tag{A17}$$

we get a system of equations

$$\begin{aligned}x(E-E_s) &= Vy + Wz, \\ y &= (R_e - i\pi\rho_e)(1+Vx), \\ z &= (R_q - i\pi\rho_q)Wx.\end{aligned} \tag{A18}$$

Solving it, we obtain

$$y = \frac{(R_e - i\pi\rho_e)(E-E_s-(R_q-i\pi\rho_q)W^2)}{E-E_s-(R_q-i\pi\rho_q)W^2-(R_e-i\pi\rho_e)V^2} \tag{A19}$$

and thus the photoconductivity spectrum

$$I(\epsilon) = \rho_e T_e^2 \frac{(\epsilon+q)^2+\gamma}{\epsilon^2+1}, \tag{A20}$$

where

$$\begin{aligned}\Gamma/2 &= \pi\rho_q W^2 + \pi\rho_e V^2, \\ \epsilon &= \frac{E-E_s-R_eV^2-R_qW^2}{\Gamma/2}, \\ q &= \frac{R_eV^2}{\pi\rho_q W^2+\pi\rho_e V^2}, \\ \gamma &= \frac{\rho_q W^2}{\rho_q W^2+\rho_e V^2} + \frac{\rho_q R_e^2 V^2 W^2}{\pi^2\rho_e(\rho_q W^2+\rho_e V^2)^2}.\end{aligned} \tag{A21}$$

This expression can be simplified if we assume that both continua have the same nature implying that $V \approx W$ and $\rho_q \gg \rho_e$. The latter follows from the fact that the $\hat{T}_e$ operator transforms an electron/hole from the ground state $|g\rangle$ to the continuum $|e\rangle$ states with the orbital momentum $l=1$, which is only a small fraction of all possible states of the charge carriers in the conduction/valence band interacting with the localized $|s\rangle$ level. Moreover, since LVMs considered here are located well above the bottom of the conduction band $R_e \ll \rho_e \ll \rho_q$. With these assumptions, we obtain that

$$q \approx 0, \quad \gamma \approx 1 + q^2\frac{\rho_q}{\rho_e} \gg q. \tag{A22}$$

It leads us to an important conclusion that Fano resonances due to LVMs of electrically active defects should have a positive sign over the background and reveal a slightly distorted Lorentzian shape.

Our conclusions agree with the experimental findings (see Table I). Moreover, from Eq. (A22), we obtain that $\rho_e/\rho_q \approx 10^{-3}$, which is consistent with our suggestion and gives us further confidence in our approach.

APPENDIX B: ABSORPTION

In this case, the light can be absorbed by both a localized state of the impurity and via excitation of an electron/hole from the bound state into the conduction/valence band. In addition to $\hat{T}_e$, a transition operator $\hat{T}_s$ from the ground to the localized $|s\rangle$ state is introduced (see Fig. 6).

Following the formalism described above after straightforward but somewhat tedious calculations, we obtain that the absorption/scattering spectrum can be formally described with the same expression as Eq. (A20), where the ϵ, Γ, q, and γ parameters are now

$$\begin{aligned}\Gamma/2 &= \pi\rho_q W^2 + \pi\rho_e V^2, \\ \epsilon &= \frac{E-E_s-R_eV^2-R_qW^2}{\Gamma/2}, \\ q &= \frac{R_eV^2+T_sV/T_e}{\pi\rho_q W^2+\pi\rho_e V^2}, \\ \gamma &= \frac{\rho_q W^2}{\rho_q W^2+\rho_e V^2} + \frac{\rho_q W^2(R_eV+T_s/T_e)^2}{\rho_e\pi^2(\rho_q W^2+\rho_e V^2)^2}.\end{aligned} \tag{B1}$$

Note that in the case of pure absorption, $T_e = 0$, we get the usual Lorentzian line shape with

$$\int_{-\infty}^{\infty} I(E)dE = T_s^2. \tag{B2}$$

It is interesting to compare the photoconductivity (subscript *pc*) and absorption (subscript *abs*) spectra of the same donor. Of main interest are parameters Γ, q, and γ. After simple transformations, we get that

$$\begin{aligned}\Gamma_{abs} &= \Gamma_{pc}, \\ q_{abs} &= q_{pc}\left(1+\frac{T_s}{T_eR_eV}\right) = q_{Ph} + \frac{T_s}{T_e}\frac{V}{\Gamma/2}, \\ \gamma_{abs}-\gamma_{pc} &= \frac{\rho_q W^2}{\pi^2\rho_e(\rho_q W^2+\rho_e V^2)^2} \\ &\quad\times\left[\left(R_eV+\frac{T_s}{T_e}\right)^2 - (R_eV)^2\right].\end{aligned} \tag{B3}$$

[1]M. Stavola and W. B. Fowler, J. Appl. Phys. **123**, 161561 (2018).
[2]S. G. Koch, E. V. Lavrov, and J. Weber, Phys. Rev. Lett. **108**, 165501 (2012).
[3]E. V. Lavrov, F. Herklotz, and J. Weber, Semicond. Sci. Technol. **30**, 024004 (2015).
[4]E. V. Lavrov, T. Mchedlidze, and F. Herklotz, J. Appl. Phys. **120**, 055703 (2016).
[5]E. V. Lavrov, I. Chaplygin, and T. Mchedlidze, Appl. Phys. Lett. **110**, 132102 (2017).
[6]U. Fano, Phys. Rev. **124**, 1866 (1961).

[7]C. G. Van de Walle, Phys. Rev. Lett. **85**, 1012 (2000).
[8]E. V. Lavrov, J. Weber, F. Börrnert, C. G. Van de Walle, and R. Helbig, Phys. Rev. B **66**, 165205 (2002).
[9]E. V. Lavrov, F. Herklotz, and J. Weber, Phys. Rev. B **79**, 165210 (2009).
[10]F. Herklotz, E. V. Lavrov, and J. Weber, Physica B **404**, 4349 (2009).
[11]E. V. Lavrov, Physica B **404**, 5075 (2009).
[12]D. G. Thomas and J. J. Lander, J. Chem. Phys. **25**, 1136 (1956).
[13]H. Y. Fan, Rep. Prog. Phys. **19**, 107 (1956).
[14]W. S. Baer, Phys. Rev. **154**, 785 (1967).
[15]A. R. Hutson, Phys. Rev. **108**, 222 (1957).
[16]R. E. Dietz, J. J. Hopfield, and D. G. Thomas, J. Appl. Phys. **32**, 2282 (1961).
[17]W. L. Bond, J. Appl. Phys. **36**, 1674 (1965).
[18]S. G. Koch, E. V. Lavrov, and J. Weber, Phys. Rev. B **89**, 235203 (2014).
[19]In fact, this maybe the very same continuum, but not taking part in photocurrent, i.e., due to the "wrong" polarization of the incoming light. Another possibility could be the electrically inactive phonon bath.
[20]A. Nitzan, Mol. Phys. **27**, 65 (1974).
[21]"Topics in applied physics," in *Light Scattering in Solids I*, edited by M. Cardona (Springer, Berlin, 1983), Vol. 8.
[22]M. Lannoo and J. Bourgoin, *Point Defects in Semiconductors I* (Springer-Verlag, Berlin, Heidelberg, New York, 1981).
[23]E. N. Economou, "Solid-state sciences," in *Green's Functions in Quantum Physics*, 3rd ed. (Springer-Verlag, Berlin, Heidelberg, 2006), Vol. 7.
[24]E. Janzén, G. Grossmann, R. Stedman, and H. G. Grimmeiss, Phys. Rev. B **31**, 8000 (1985).